ORNL/TM-2022/2505

Feasibility Study of Spectrophotometry to Support a Promethium Production Program at ORNL

Luke R. Sadergaski
Hunter B. Andrews
Kenton Wilson
Stacy L. Queern
Riley D. Hunley

June 2022

Approved for public release.

OAK RIDGE National Laboratory

ORNL IS MANAGED BY UT-BATTELLE LLC FOR THE US DEPARTMENT OF ENERGY

ORNL/TM-2022/2505

Radioisotope Science and Technology Division

Feasibility Study of Spectrophotometry to Support a Promethium Production Program at ORNL

Luke R. Sadergaski
Hunter B. Andrews
Stacy L. Queern
Riley D. Hunley

June 2022

Prepared by
OAK RIDGE NATIONAL LABORATORY
Oak Ridge, TN 37831-6283
managed by
UT-BATTELLE, LLC
for the
US DEPARTMENT OF ENERGY
under contract DE-AC05-00OR22725

CONTENTS

FIGURES

TABLES

ABBREVIATIONS

CV	cross validation
HFIR	High Flux Isotope Reactor
ICP-OES	inductively coupled plasma–optical emission spectrometry
LOD	limit of detection
LOQ	limit of quantification
ORNL	Oak Ridge National Laboratory
PLSR	partial least-squares regression
RMSEC	root-mean square error of the calibration
RMSECV	root-mean square error of the cross validation
TODGA	N,N,N′,N′-Tetraoctyl diglycolamide
UV-Vis-NIR	Ultraviolet-Visible-Near Infrared

ACKNOWLEDGMENTS

The authors wish to thank Richard T. Mayes and Laetitia H. Delmau for help with acquiring a promethium sample. Funding for this work was provided by the US Isotope Program. This work used resources at the Radiochemical Engineering Development Center operated by Oak Ridge National Laboratory.

ABSTRACT

Optical spectroscopy can be used to optimize analytical measurements for lanthanide elements and provide real-time feedback to help guide production operations. This study evaluates spectrophotometry for the determination of samarium (Sm^{3+}) and neodymium (Nd^{3+}) in aqueous and organic solutions at concentrations relevant to a promethium (Pm) program separation scheme. Detection limits approached 0.5 mM for Nd^{3+} and 2 mM for Sm^{3+} using Ocean Insight spectrophotometers. Additionally, Sm^{3+} detection limits using laser fluorescence spectra for Sm^{3+} approached single ppm ($mg \cdot L^{-1}$) levels. An absorption spectrum containing Nd and Pm is also reported and discussed. This work demonstrates proof-of-principle concepts for applying spectrophotometry to online monitoring applications in support of a future Pm production program.

1. BACKGROUND AND MOTIVATION

1.1 OPTICAL SPECTROSCOPY

Optical spectroscopy is useful for monitoring radiochemical separations in-line from lab- to industrial-scale applications. Spectrophotometry, or absorption spectroscopy, quantitatively measures the amount of light absorbed by a molecule as a function of wavelength. Absorbance is proportional to the concentration of a light-absorbing species and can be quantified using Beer's law. Spectral response in an absorption spectrum is linear (i.e., univariate) when the solute is sufficiently dilute and quantified when the optical pathlength and molar absorptivity of a substance is known. When the univariate approach breaks down in complex systems with overlapping absorption bands, shifting baselines, and dependencies on solution conditions, multivariate data analysis (e.g., partial least-squares regression [PLSR]) can be used to describe complex systems. PLSR correlates the entire spectrum (instead of a single wavelength) to the concentration of species in solution.

Fiber-optic cables can transmit light over large distance (e.g., hundreds of meters) to enable ultraviolet/visible/near infrared (UV-Vis-NIR) absorption measurements in hot cells while personnel operate equipment in a control room. This allows spectroscopic measurements of materials located in the hot cells at the Radiochemical Engineering Development Center at Oak Ridge National Laboratory (ORNL) without transferring samples out of the cells for the ^{238}Pu Supply Program at ORNL [1–6]. The developed approach can readily be adapted to other isotope production programs [7].

UV-Vis-NIR absorption spectroscopy can provide operational benefits to radioisotope production operations in a hot cell, including little or no sample dilution, no sample transfer, real-time process feedback for performance optimization, and enhanced sensitivity. UV-Vis-NIR spectrometers collect spectra at rapid intervals (e.g., 10 ms–1,000 ms) and contain a wealth of information. The data are more intuitive for users to understand when converted to process variables, such as concentration. Converting spectra to process variables in real time assists users monitoring complex systems and can be implemented using an online monitoring software [4].

1.2 MOTIVATION

The US DOE's Isotope Program is investing in the production of Pm^{3+}, a valuable radioisotope for numerous applications (ref or example?). An option for producing this rare isotope is by irradiating Nd^{3+} at the High Flux Isotope Reactor (HFIR) at ORNL. After irradiation, the ^{147}Pm must be separated from Nd and purified, while Nd is recycled to produce more Pm in subsequent cycles. In addition to these lanthanides, daughter Sm^{3+} isotopes will also be present in this system.

Each lanthanide species (i.e., Nd, Pm, Sm) absorbs light in the UV-Vis-NIR region of the electromagnetic spectrum [8–10]. Each element is also fluorescent, although the quantum yield of Sm^{3+} in the visible region makes it much more sensitive—down to single ppm concentration levels. Dual absorption and fluorescence cells could be applied to simultaneously monitor Sm and Nd/Pm, respectively. Nd and Pm fluoresce occurs near the NIR region where non-photoemission collisional mechanisms for deexcitation are more probable than spontaneous emission back to ground state. However, with the appropriate setup, it is still a conceivable option. The operational benefits afforded by employing optical spectroscopy are worth the upfront investment.

Here we demonstrate proof-of-principle concepts for online monitoring capabilities and analytical measurements using spectrophotometry. These are expected to increase the timeliness of analytical measurements and help guide decisions during radiochemical processing. Detection limits for Nd and Sm

and reference spectra are reported with different instruments. A Pm spectrum, convoluted with Nd peaks, is also presented and to accommodate a discussion regarding measurements with varying isotopic compositions. Finally, areas for advanced optical techniques and interesting research and development are provided in the final chapter.

2. TESTING WITH THE CARY 6000I

2.1 MATERIALS

The Cary 6000i is a double-beam UV-Vis-NIR spectrophotometer made by Agilent. It can cover a wide range of wavelengths (175–1,800 nm). The spectral bandwidth of the instrument varies from 0.01 to 5 nm (UV-Vis) and 0.04 to 20 nm (NIR), depending on the instrument settings. Spectra were recorded using a standard Cary 6000i configuration and a static 1 cm quartz cuvette (Figure 2.1). Fiber-based measurements are also a possibility using the Fiber-mate accessory (not shown here). The Cary 6000i is on a mobile cart that can be wheeled to multiple locations per RSS 19212.

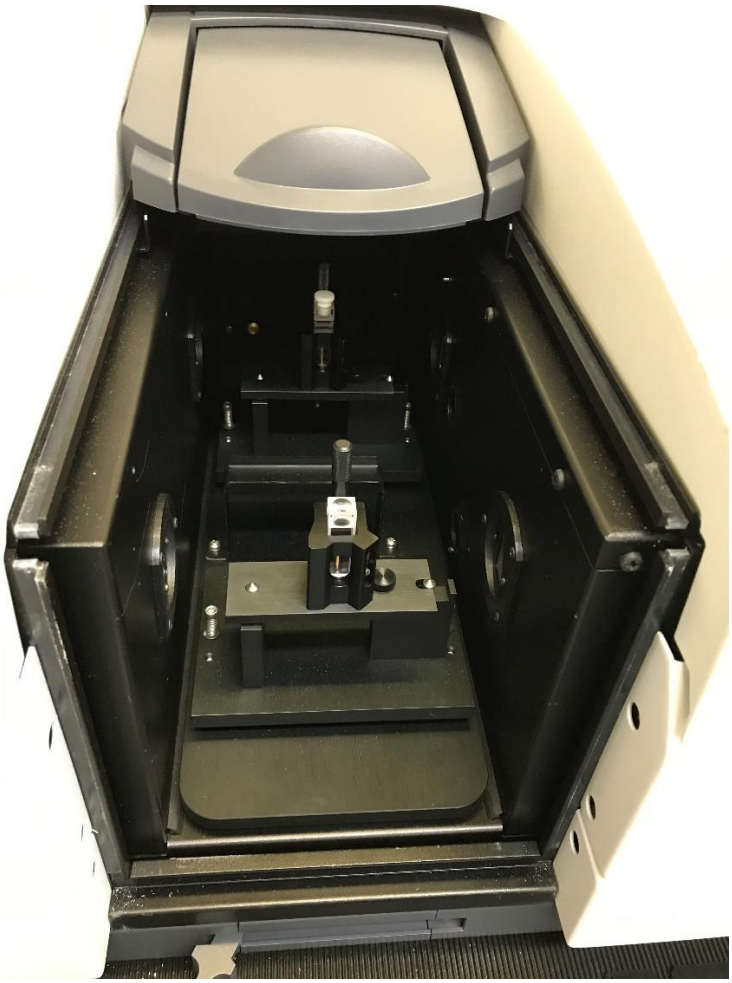

Figure 2.1. Cary 6000i physical setup in Lab 110.

2.2 Nd^{3+} CALIBRATION CURVE

Vis-NIR absorption spectra corresponding to various Nd^{3+} concentrations (0.48–50 mM) are shown in Figure 2.2. These were prepared by diluting an inductively coupled plasma–optical emission spectrometry (ICP-OES) stock solution (10,000 ppm) in water. Samples were pipetted in and out of a 1 cm quartz cuvette. Nd^{3+} ions absorb light at many frequencies from ~500 to 950 nm, and the peaks tend to follow Beer's law (i.e., absorbance increases linearly with increasing concentration). These spectra were recorded using a step size of 2 nm and an integration time of 0.033 s. An entire spectrum was recorded in ~50 s.

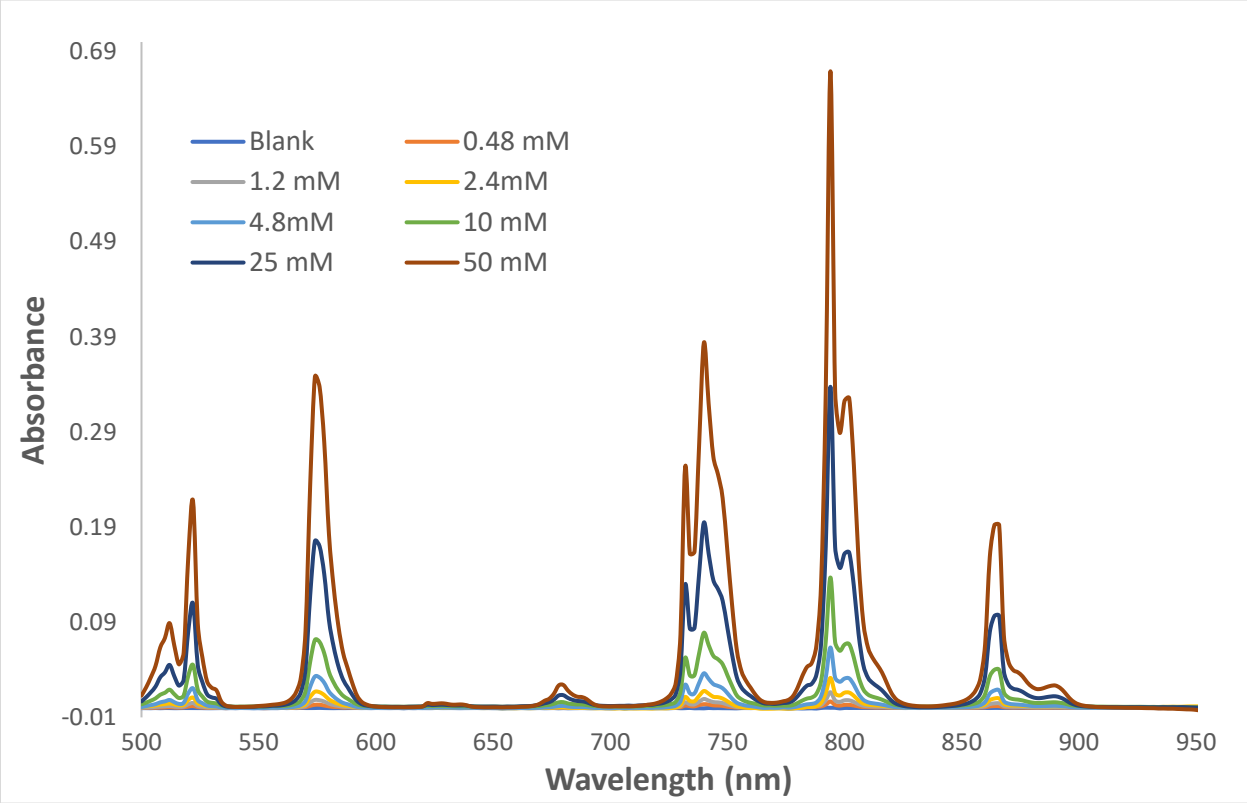

Figure 2.2. Vis-NIR absorption spectra of Nd^{3+} calibration samples in nitric acid.

Higher-resolution scans are possible but may not be necessary (Figure 2.3). This will depend on the intended application(s). Higher-resolution scans will increase the time it takes to record a measurement. The scan rate could be improved significantly by scanning a smaller portion of the spectrum (e.g., 790–800 nm).

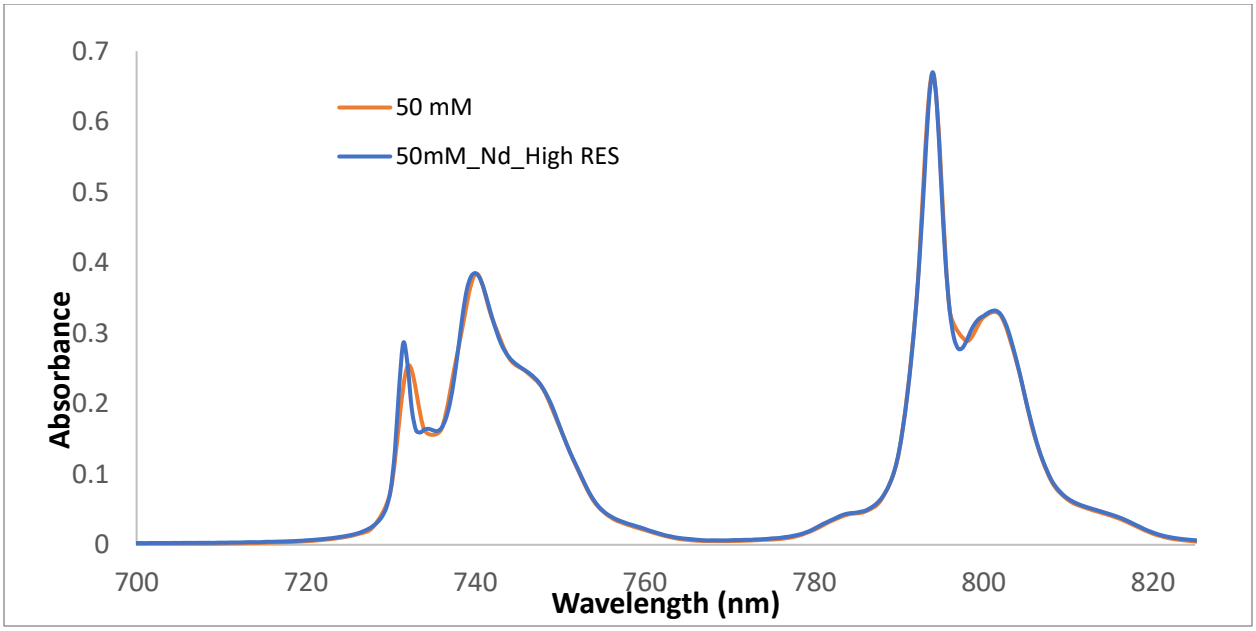

Figure 2.3. Vis-NIR spectra of a 50 mM solution using a 2 nm step size (orange) and a 0.5 nm step size (blue).

The absorption peaks at 794 and 574 nm are useful for quantitative Nd^{3+} concentration determinations (Figure 2.4). Both linear regressions had immaculate correlation values. The molar extinction for the most intense peak at 794 nm was calculated to be 13.5 ± 0.3 $M^{-1}{\cdot}cm^{-1}$, and the peak at 574 nm had a coefficient of 6.95 ± 0.1 $M^{-1}{\cdot}cm^{-1}$. Either the regression or molar extinction coefficient value could be used for quantitative analysis.

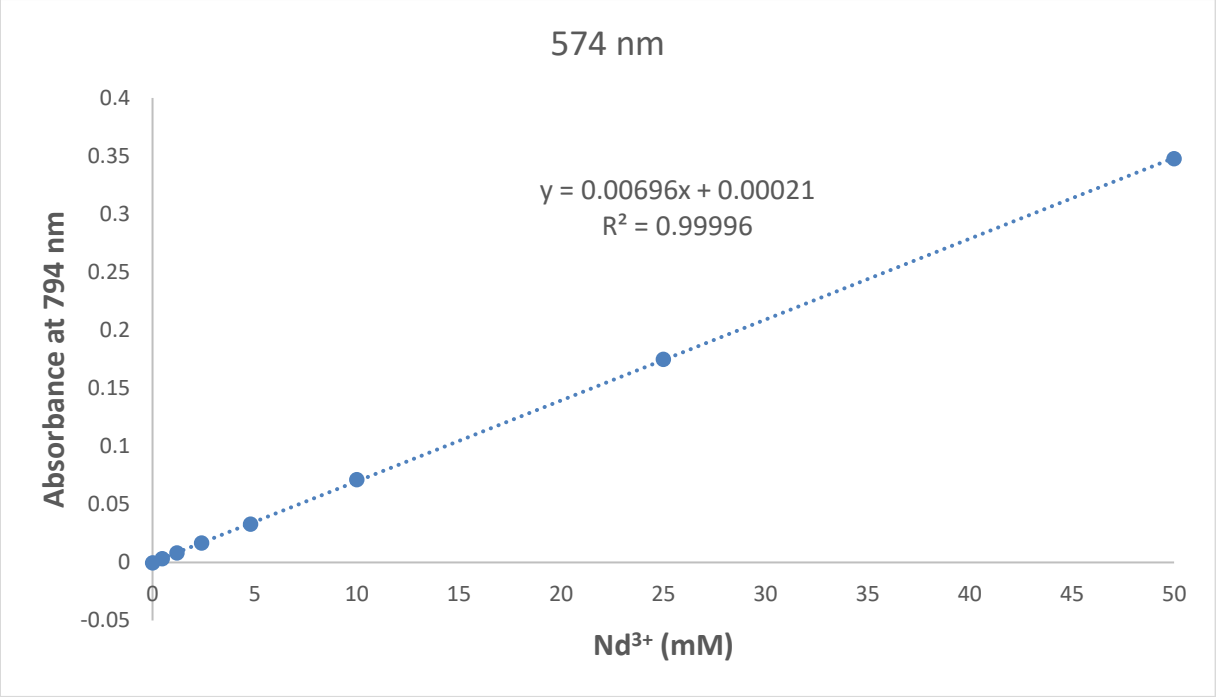

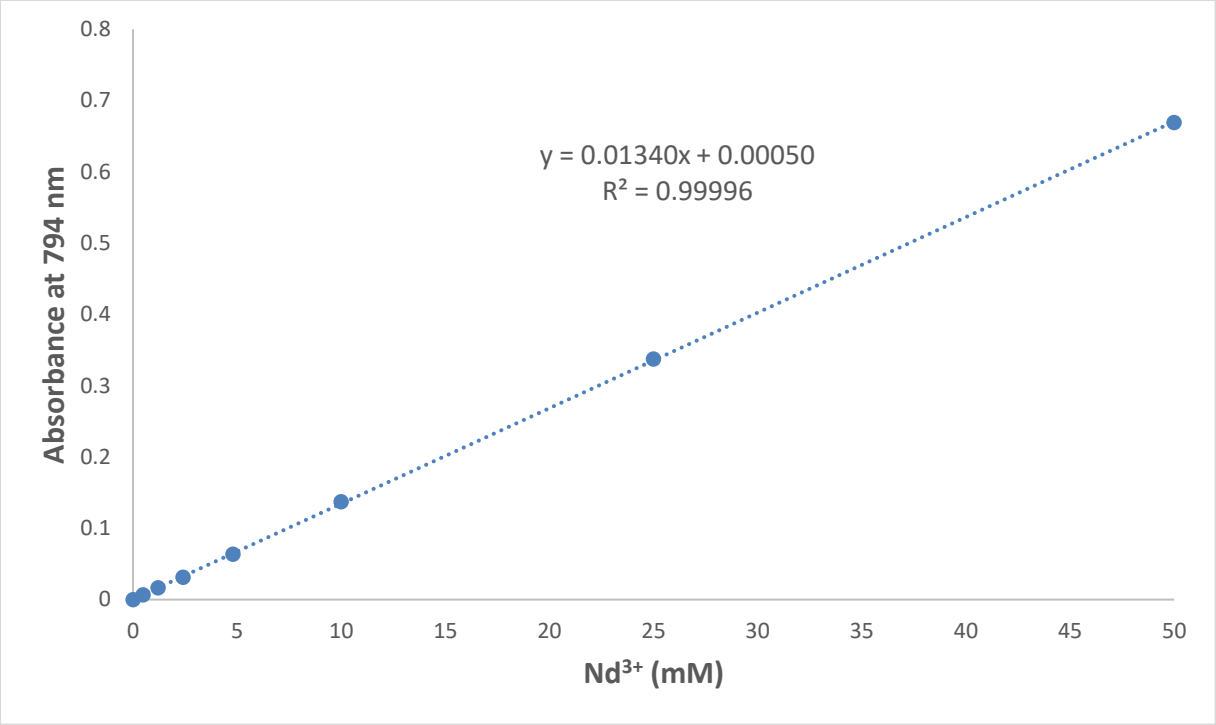

Figure 2.4. Linear regression of the 574 nm peak (top) and 794 nm peak (bottom) intensity vs. Nd^{3+} concentration.

2.3 Nd^{3+} LIMITS OF DETECTION

Univariate linear regressions describing the relationship between Nd^{3+} concentration and the 794 nm and 574 nm Nd^{3+} absorption bands were used to determine detection limits. Regression data takes the form $y = mx + b$. The limit of detection (LOD) and limit of quantification (LOQ) were calculated by $LOD = 3\sigma_b/m$ and $LOQ = 10\sigma_b/m$, where b represents the intercept, σ_b is the standard deviation of the intercept, and m is the slope of the line. OriginPro software was used to determine the standard deviation of the intercept.

The calculated LOD and LOQ for the 794 nm peak with the configuration, instrument settings, and data shown here are 0.18 mM and 0.61 mM Nd^{3+}, respectively. The calculated LOD and LOQ for the 574 nm peak with the configuration, instrument settings, and data shown here are 0.17 mM and 0.56 mM Nd^{3+}, respectively. Although the 574 nm peak intensity was less than the 794 nm peak, it resulted in slightly better detection limits. The 574 nm band may be less sensitive to fluctuations in acid concentration, which ranged from near zero to ~5% HNO_3 in this data set. Future tests should be completed at constant acid concentration, comparable to the way calibration standards are prepared for ICP-OES measurements.

2.4 SUMMARY OF INITIAL FINDINGS USING THE CARY 6000I

Absorption spectrophotometry can be used to quantify Nd^{3+} concentrations ≤~0.5 mM using a 1 cm optical pathlength and the Cary 6000i spectrophotometer. Spectral data in this summary were not preprocessed in any way. However, data preprocessing could improve detection limits by improving the relationship between spectra and concentration. A quartz flow 1 cm cuvette could also improve detection limits and reproducibility because the position of the cell would remain completely fixed. The sample could be introduced in and out of the cell using a syringe. Finally, maintaining a constant acid concentration, using a longer optical pathlength, or changing the spectral resolution could also further

improve detection limits. Future testing could compare data acquired using the main sample compartment to remote measurements using the fiber launch module. Longer pathlength options for the main sample compartment holders are available at a reasonable cost from Agilent. Longer pathlength quartz cuvettes (e.g., 5 cm) are also available if lower detection limits are desired.

3. MIXER–SETTLER TESTING IN THE MAKEUP AREA

3.1 FIRST-RUN RESULTS

Dip probes were placed in the various stages of the mixer–settler bank in the makeup area to acquire absorption spectra. Two dip probes were used during the first mixer–settler run (Figure 4.1). They were placed in distinct locations to determine whether Sm was being extracted into the organic phase and Nd was in the raffinate.

Figure 4.1. Avantes (1 cm) and Hellma Vis-NIR dip probes (1 cm) placed in the aqueous phase of Stage 8 and Stage 13, respectively.

They were used to monitor both the aqueous and organic phase (Figure 4.2). It would be advantageous to develop a sleeve with a stopper to hold the probe in the organic phase, so the probe toned not be held. Ocean Insight spectrophotometers (QEPro and NIRQuest) were used to record the data.

Figure 4.2. Hellma Vis-NIR dip probe (1 cm) placed in the organic phase (left) and the aqueous phase (right).

3.1.1 Organic-Phase Reference Spectrum

Reference organic-phase spectra of Sm^{3+} (13.5 mM) and Nd^{3+} (4.23 mM) is shown in Figure 4.3. Epsilon values for each peak are provided in Table 4.1. The primary Sm^{3+} and Nd^{3+} peaks are labeled. The Sm peaks appeared near 404 and 1,090 nm, and the Nd peaks were located at 584 and 801 nm. The 404 nm Sm peak in the organic phase is shifted compared to the aqueous phase at 401 nm. Peaks for each species are clearly distinguishable and were not convoluted. Thus, it is appropriate to apply Beer's law for quantification in this instance.

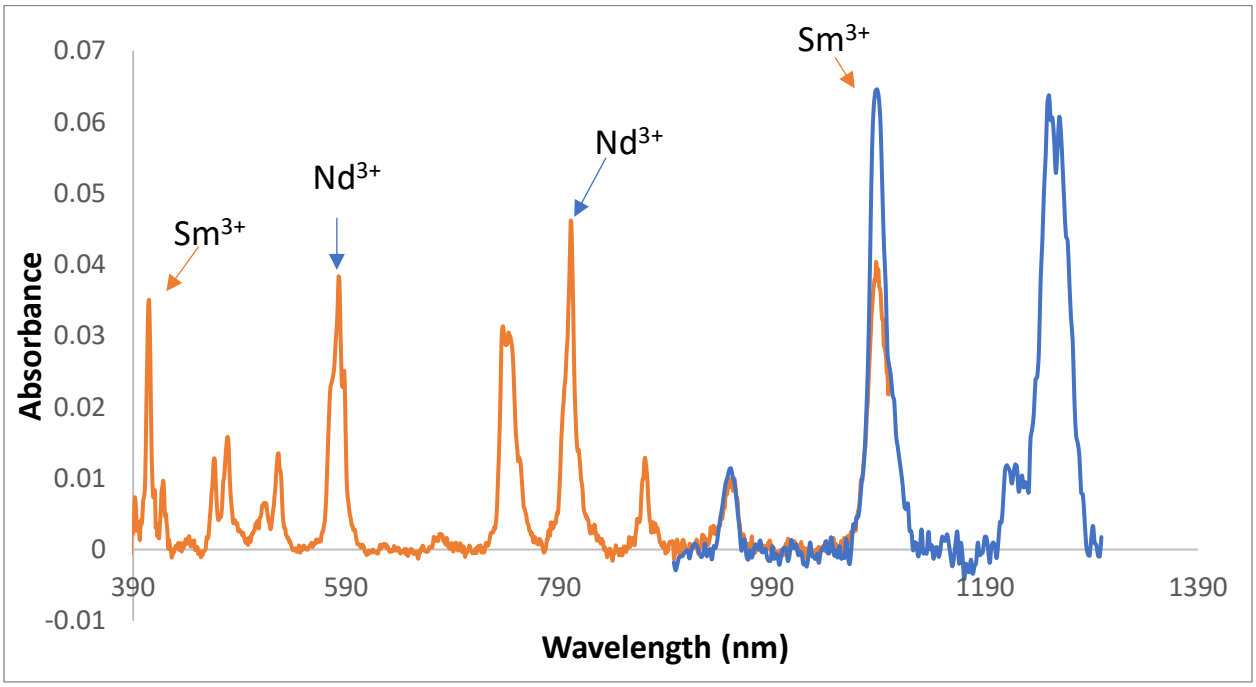

Figure 4.3. Vis-NIR absorption spectra with primary Sm^{3+} and Nd^{3+} peaks labeled.

Table 4.1. Epsilon ($M^{-1} \cdot cm^{-1}$) values for each peak.

Species	Peak nm	Epsilon
Sm^{3+}	1,090	4.9
	404	2.5
Nd^{3+}	801	10.3
	854	8.9

3.1.2 Grab Samples

The feed for the first mixer–settler run was composed of nearly equal concentrations (25 mM) of Sm and Nd. Grab samples were taken during the run for analysis by spectrophotometry and ICP-OES using a static 1 cm small volume cuvette shown in Figure 4.4. A comparison of the two techniques will be provided in a separate report.

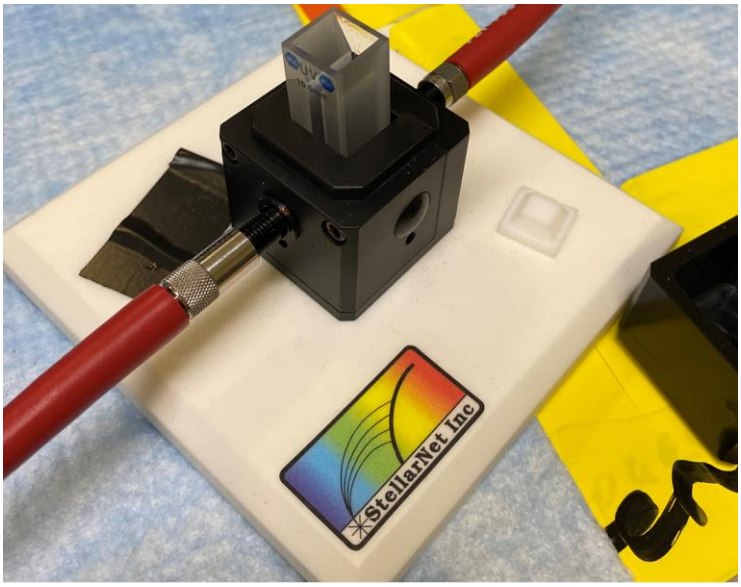

Figure 4.4. Cuvette (10 mm) and cuvette holder in Lab 110.

3.1.3 Stage Profiles

This section provides example organic-phase concentration profiles in various stages of the mixer–settler bank. We acquired bank profiles with the 10 mm NIR Hellma dip probe in the organic and aqueous phases. Spectra were collected at <1 s intervals. Sm^{3+} was measurable in Stages 3–16. The concentrations were measured using the 1,089 nm peak at a molar epsilon value of 4.9. Figure 4.5 shows organic-phase spectra for Sm in Stages 4–11, and Table 4.2 provides concentration values for Sm in organic-phase Stages 1–16.

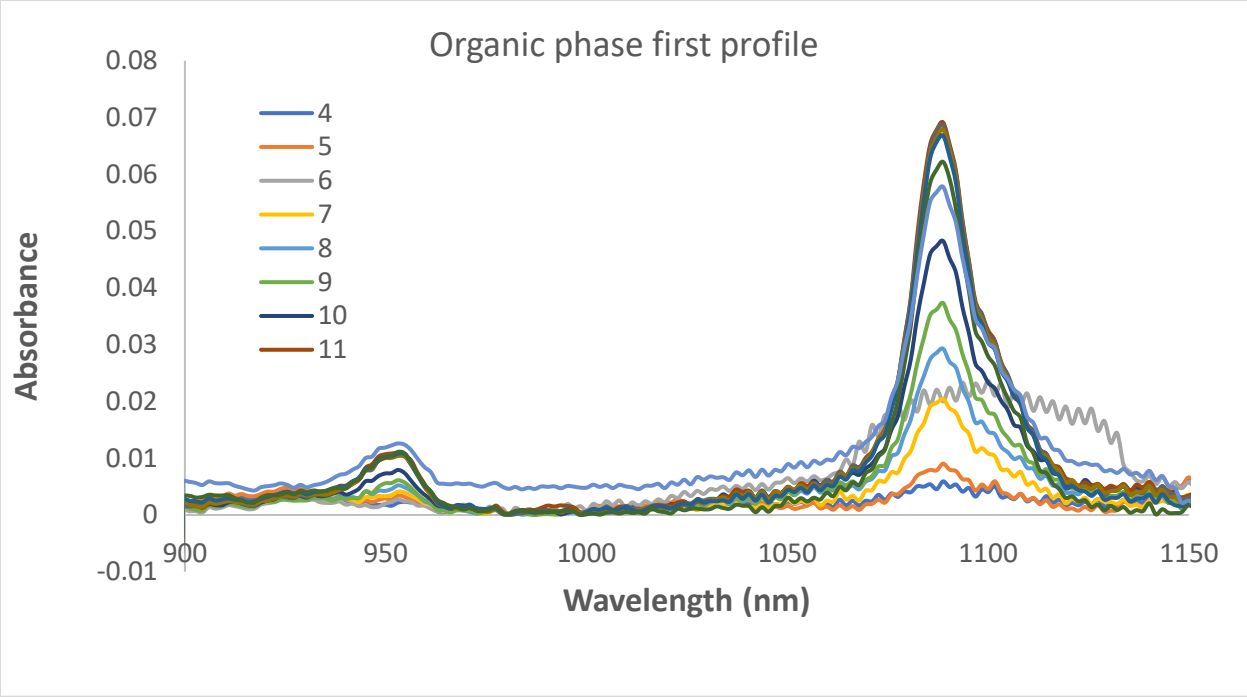

Figure 4.5. Organic-phase Sm^{3+} spectra in Stages 4–11.

Table 4.2. Concentration of Sm measured in the organic-phase Stages 1–16.

Stage	1,088.796	Sm mM
1	0.004128	0.00
2	0.00309	0.00
3	0.003181	0.00
4	0.005924	1.2
5	0.009044	1.8
6	0.02	4.1
7	0.020417	4.2
8	0.029283	6.0
9	0.037332	7.6
10	0.048258	9.8
11	0.069157	14.1
12	0.068731	14.0
13	0.067915	13.9
14	0.066807	13.6
15	0.062192	12.7
16	0.057805	11.8

Obtained measureable Nd concentration values in Stages 9–16 of the organic phase. The amount of Nd in Stage 9 was lower than quantification limits. The 800 nm peak was used to obtain Nd concentration in the organic phase using a 10.3 epsilon value. We did not measure Nd in the organic phase Stages 1–8. Figure

4.6 shows organic-phase spectra for Nd in Stages 9–16, and Table 4.3 provides concentration values for Nd in organic-phase Stages 1–16. The Sm 404 nm peak could also be used for quantification.

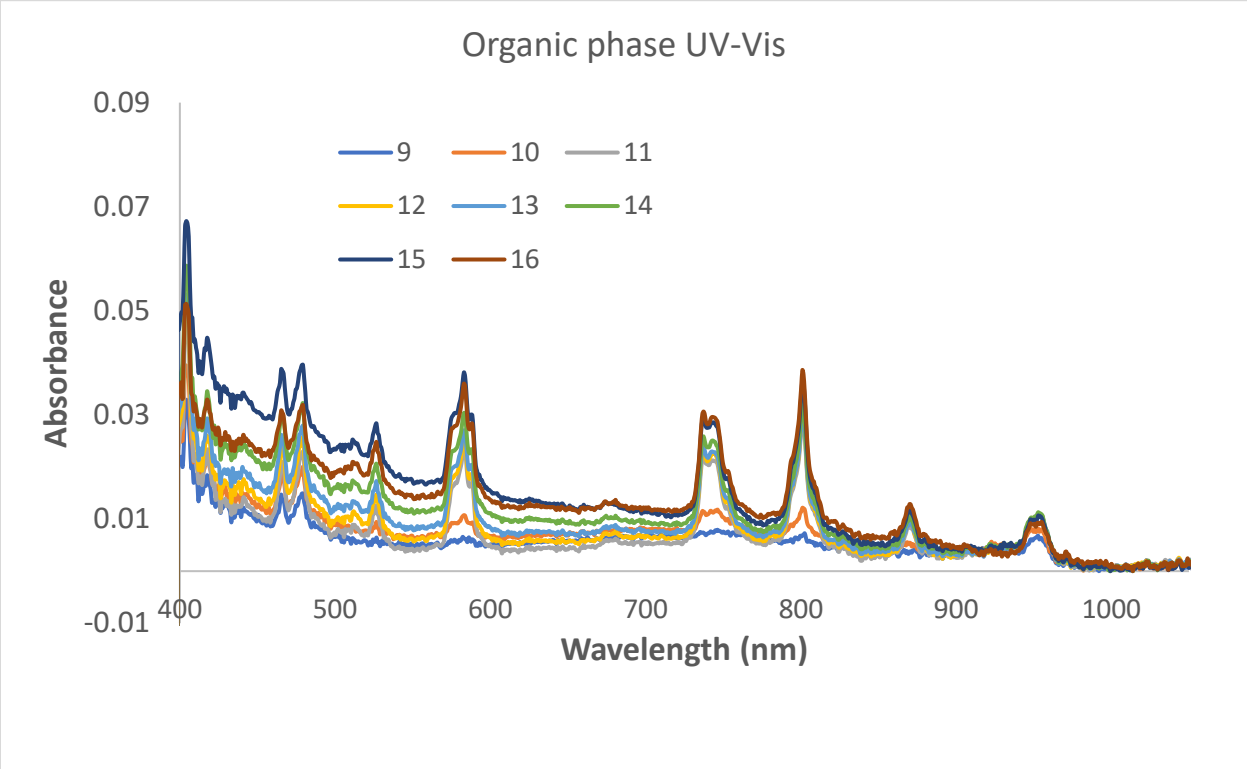

Figure 4.6. Organic-phase Nd^{3+} spectra in Stages 9–16.

Table 4.3. Concentration of Nd measured in the organic-phase Stages 1–16.

Stage	800.995	Nd mM
1	0.0011	0.00
2	0.0010	0.00
3	0.0011	0.00
4	0.0016	0.00
5	0.0009	0.00
6	0.0014	0.00
7	0.0007	0.00
8	0.0015	0.00
9	0.0027	0.27
10	0.0066	0.64
11	0.0250	2.42
12	0.0250	2.43
13	0.0245	2.38
14	0.0254	2.46
15	0.0287	2.79
16	0.0294	2.85

3.1.4 PLSR Model Development and Concentration Profiles

Stage 13 was monitored during the entire run unless the probe was being used for stage profiles. The entire data set was described using principal component analysis, and calibration samples were selected using a Kennard-Stone sample selection algorithm. This method was outlined previously [7]. These 10 samples are shown in Figure 4.7. The first derivative accounted for nonlinear baseline offset issues in the spectra better than applying a linear baseline offset correction. PLSR models built using the first derivative performed better (data not shown here).

Derivatives are useful for correcting baseline offset effects in spectra. A Savitzky-Golay algorithm was used to compute the first derivative using the Unscrambler. This algorithm takes the derivative of a polynomial (third order) fitted by a least-squares linear regression around a specified number of adjacent variables (seven points). First-order derivatives measure the rate of change of absorbance at each wavelength and pass through zero at wavelength corresponding to absorbance values of maximum intensity (peaks). Peak inflection points correspond to positive and negative peaks on either side of the zero point.

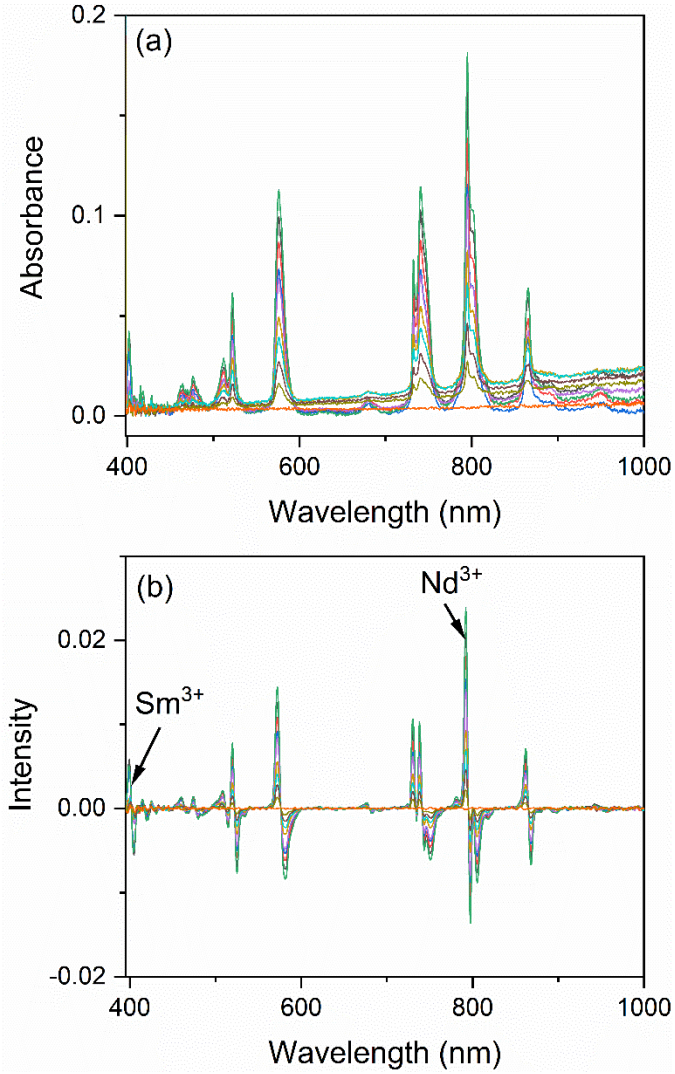

Figure 4.7. Absorption spectra used as the training set after applying (a) baseline offset correction and (b) first derivative.

Regression coefficients describe the relationship between predictors (i.e., spectra), and a given response (i.e., concentration) for any number of factors. The Sm and Nd regression coefficients for two factors are shown in Figure 4.8. Intense (nonzero) regression coefficients play a more significant role in the regression model while those close to zero provide little or no useful information for a given response. Predictors with small coefficients can be omitted from the model to improve it. In Figure 4.8 the regression coefficients with respect to Sm^{3+} "look like spectra" and give importance to the primary 401 nm peak and no importance to Nd peaks. The regression coefficients for Nd also look like a Nd^{3+} first-derivative spectrum. This shows that the PLSR model accurately describes the correct species and spectral component.

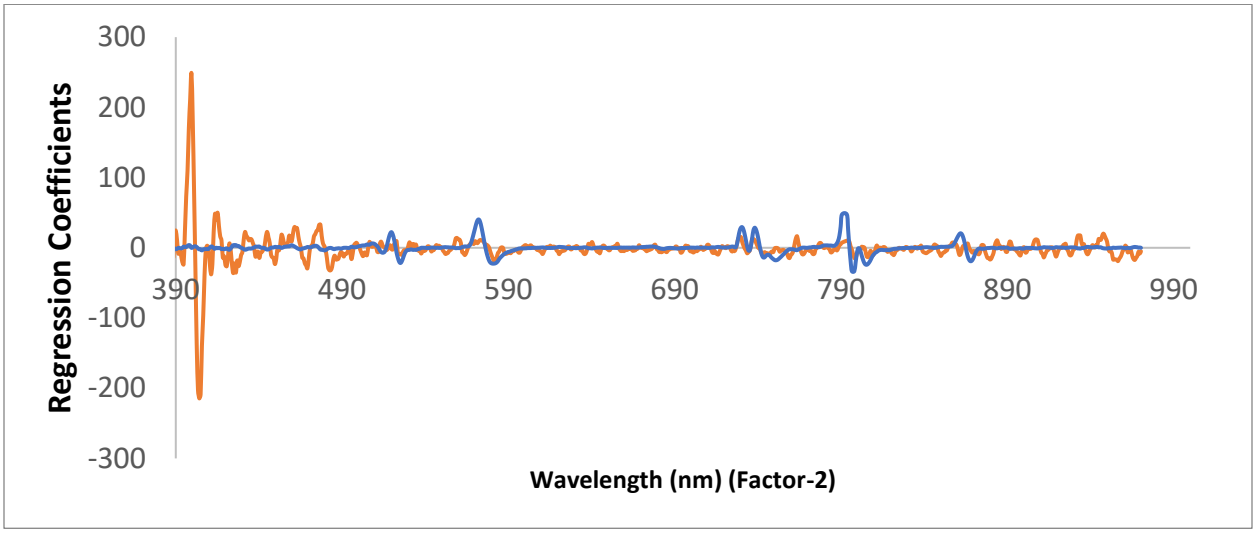

Figure 4.8. Regression coefficients for Sm^{3+} (orange) and Nd^{3+} (blue).

The root-mean square error of the calibration (RMSEC) and cross validation (RMSECV) were used to evaluate PLSR model performance. A full CV was performed by randomly taking one sample at a time from the calibration set, until every sample was left out once, and recalibrating submodels on the remaining data points. The residuals from each submodel were combined to compute the CV residual variance, which is an estimate of the residuals (i.e., uncertainty) in the root-mean square error of the predictions. The explained variance for the calibration and validation after two factors was 99.57 and 99.12%, respectively. Thus, most of the structured variation in the data set is described using two factors. Additional factors did not improve CV statistics.

Predicted Y-values were plotted against reference Y-values to check the quality of the regression model (Figure 4.9). Quality models will conform to a straight line, and RMSEC and RMSECV values will be similar. The RMSEC for Sm^{3+} improves with additional factors. However, the RMSECV did not improve, which suggests that two factors were more representative. Too many factors will result in overfitting and modeling noise. The fit for Nd^{3+} was very good because most of the samples were above limits of quantification. The molar epsilon for Nd is nearly four times greater than Sm. The Sm fit was adequate but suffered from a weak signal near the LOD. Future work using an optical pathlength of 2 cm or a 1,090 nm Sm peak in the NIR region could improve model performance at low Sm concentrations near 1 mM. This PLSR model could be used in future iterations to provide concentration information in real time.

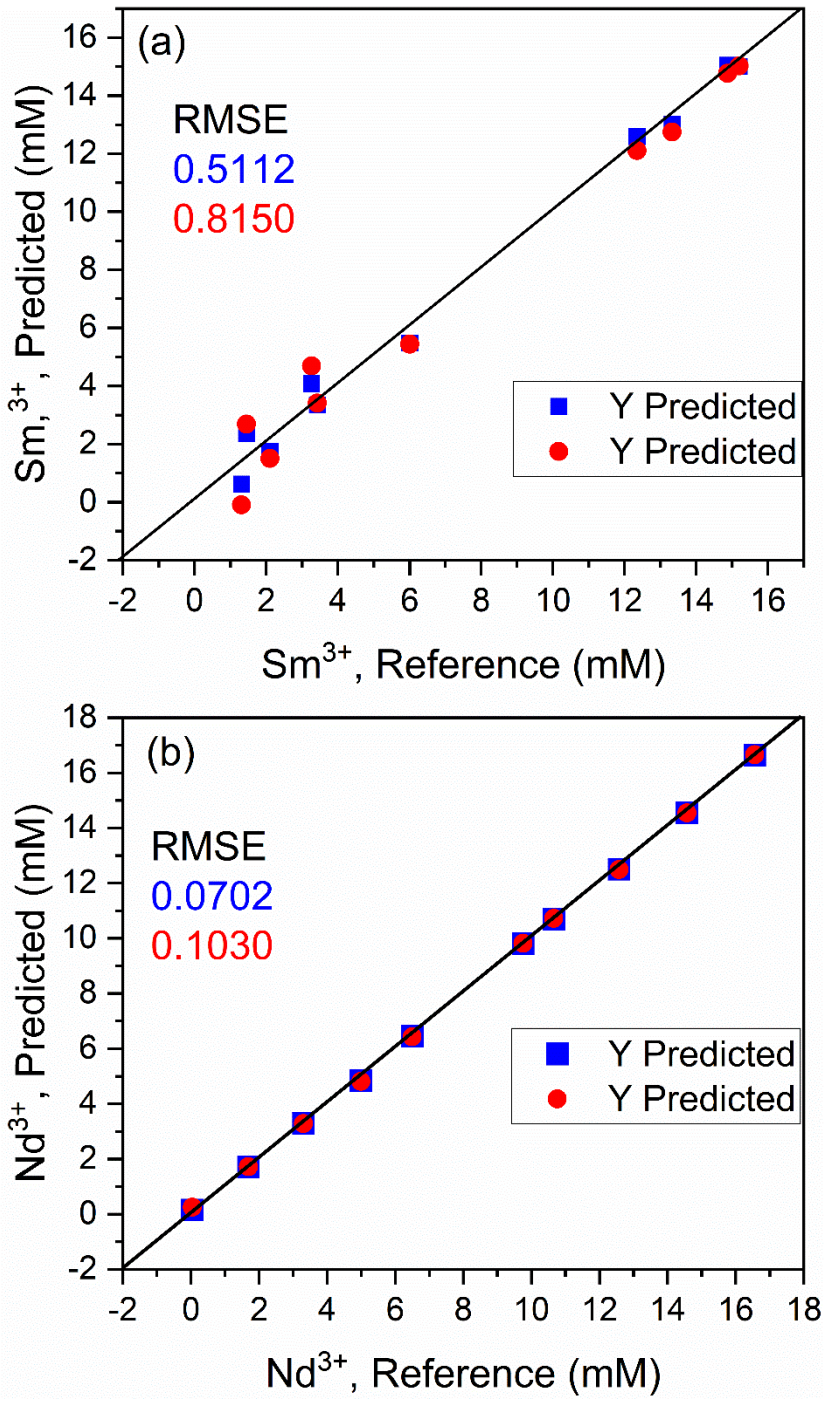

Figure 4.9. PLSR parity plots and RMSE values for calibration and cross-validation data (1) Sm^{3+} and (b) Nd^{3+}. Blue squares and red circles represent the calibration and CV data, respectively.

3.2 SECOND-RUN RESULTS

The second mixer–settler run in the makeup area of Building 7920 was operated under conditions closer to what is anticipated in a future production operation. The feed was composed of primarily Nd (~22 mM) with a much lower concentration of Sm (~0.5 mM).

3.2.1 Grab Samples

Several grab samples were taken for analysis by spectrophotometry and ICP-OES. The spectra corresponding to these samples are shown in Figure 4.10. Sm was below the limit of quantification for spectrophotometry. Nd was clearly measurable. Peak intensities and concentrations of Nd are provided in Table 4.4. The results shown here will be compared to ICP-OES in a separate report.

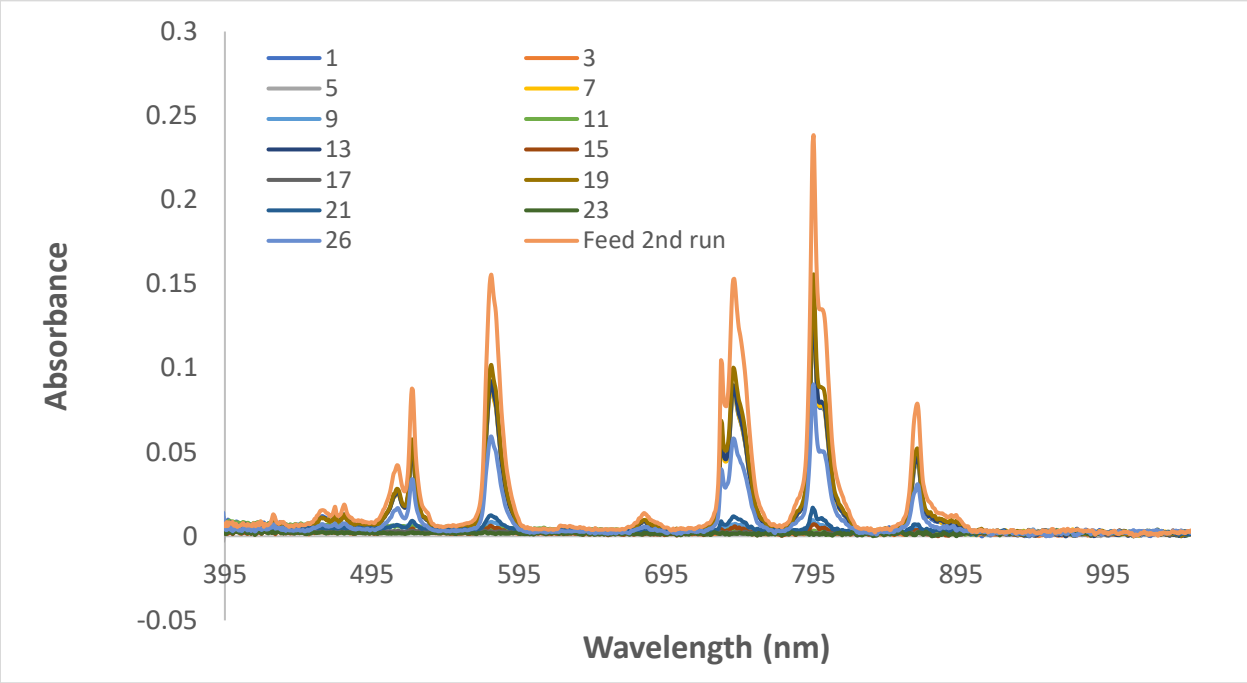

Figure 4.10. UV-Vis spectra (bottom) of each grab sample. No signal was acquired in the NIR (>900 nm) region as expected.

Table 4.4. Peak intensities and concentrations of Nd.

Sample	576.052	Nd mM	795.028	Nd mM
1	0.091	12.1	0.138	12.5
3	0.003	0.4	0.003	0.3
5	0.002	0.0	0.002	0.0
7	0.090	11.9	0.137	12.4
9	0.009	1.1	0.009	0.8
11	0.005	0.0	0.003	0.0
13	0.092	12.3	0.141	12.8
15	0.006	0.8	0.007	0.7
17	0.003	0.0	0.001	0.0
19	0.102	13.6	0.156	14.1
21	0.012	1.7	0.016	1.5
23	0.002	0.0	0.001	0.0
26	0.059	7.9	0.090	8.2
Feed	0.155	20.7	0.238	21.7

3.2.2 Stage Profiles

This section provides examples of Nd organic-phase and aqueous-phase spectra taken across multiple stages of the mixer–settler bank. Several example absorption spectra of Nd in the organic phase and aqueous phases are shown in Figure 4.11 and 4.12, respectively. The spectra span multiple stages of the mixer–settler bank and show drastic differences in spectral response that can be correlated to concentration using Beer's law. The calculated concentration profiles are shown in Figure 4.13 and 4.14. The concentrations of Nd in the organic and aqueous phases across most stages were relatively consistent during the run.

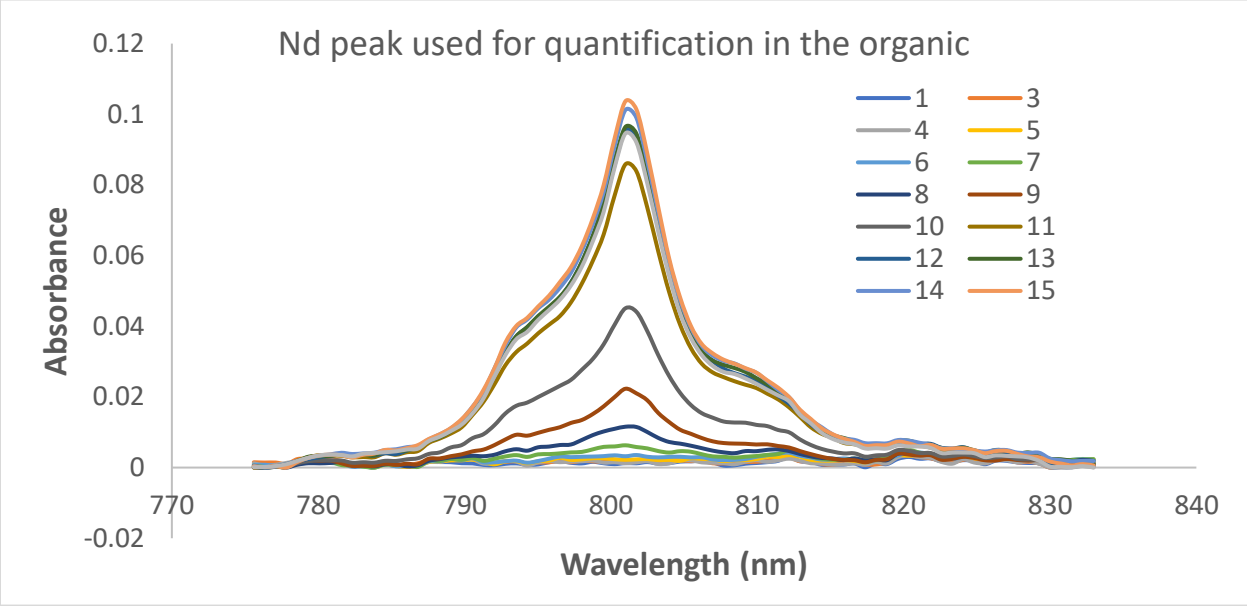

Figure 4.11. UV-Vis spectra for the organic phase in most stage positions.

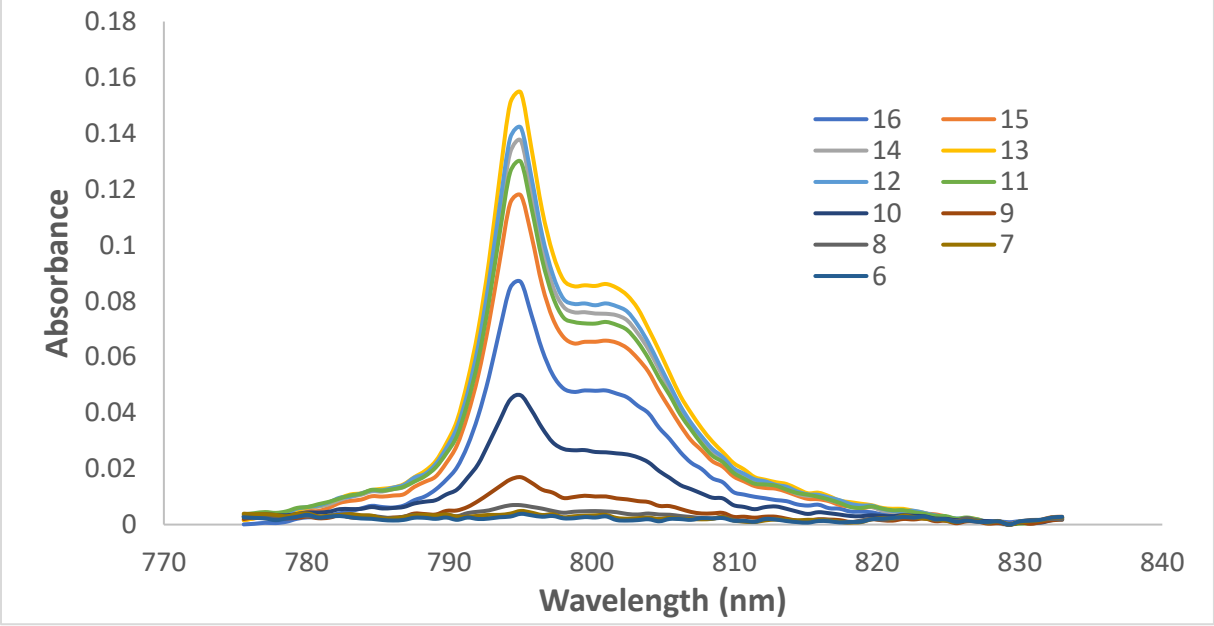

Figure 4.12. UV-Vis spectra for the aqueous phase in several stage positions.

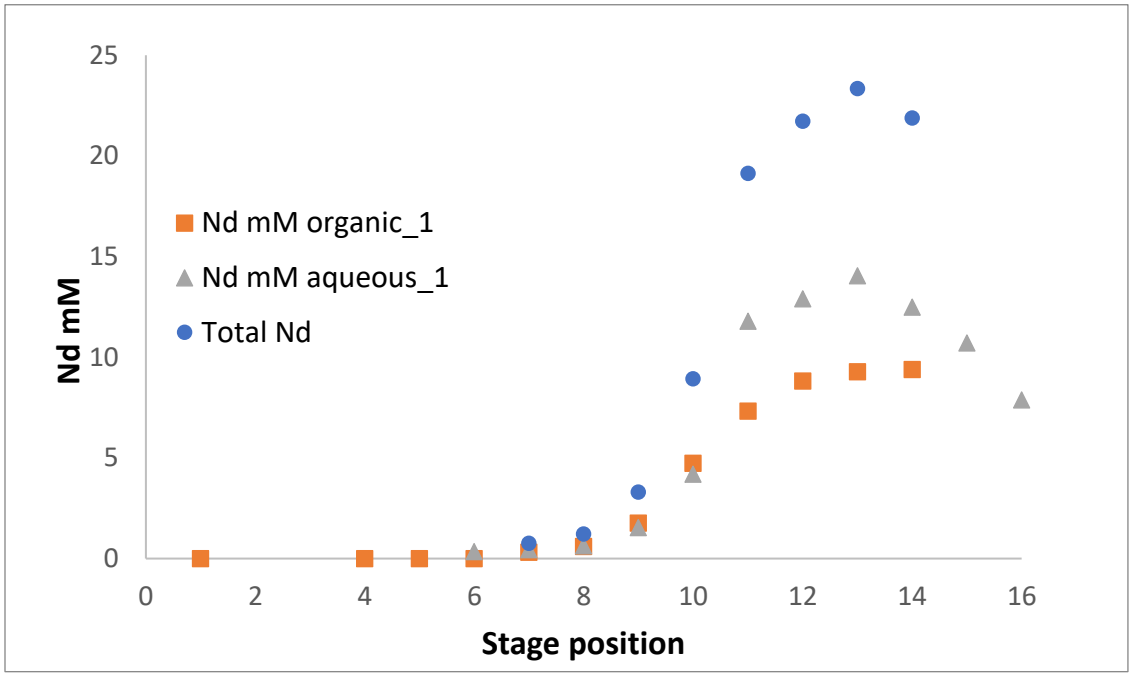

Figure 4.13. Nd concentration profile in the organic phase and aqueous phase in several stage positions (first profile at ~9:45 a.m.).

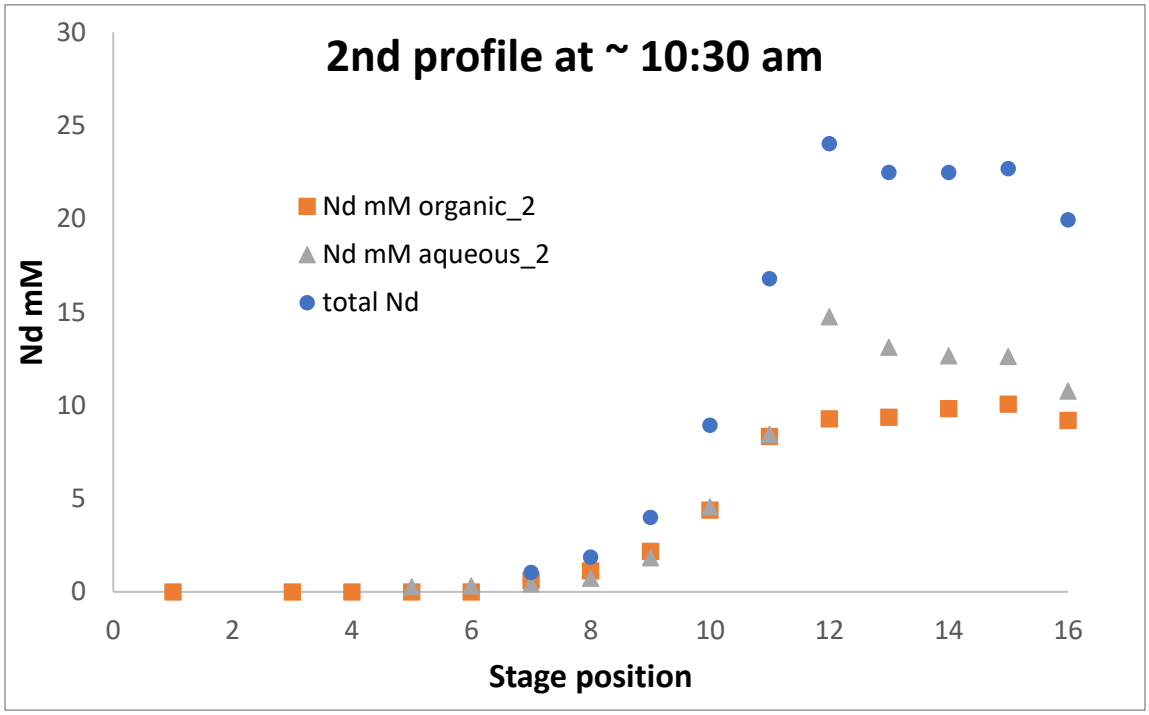

Figure 4.14. Nd concentration profile in the organic phase and aqueous phase in several stage positions (second profile at ~10:30 a.m.).

3.3 THIRD-RUN RESULTS

3.3.1 Stage Profiles

The mixer–settler run conditions were changed significantly prior to the third run. Spectrophotometry was used to identify different profiles during the run. Spectra were collected at <1 s intervals. The initial profile at ~9:30 a.m. appeared to be operating mostly as planned with respect to Sm. Table 4.5 provides concentration profiles for Sm and Nd in the 9:30 a.m. run. Sm^{3+} was primarily located in stages on the lefthand side of the bank while very little Sm^{3+} made its way to Stages 14–15. However, concentration profiles for Sm and Nd changed significantly in the 11:00 a.m. run (Table 4.6). Nd^{3+} was identified in the aqueous phase of Stages 1, 3–6 later in the run (Figure 4.16) but was not earlier in the run (Figure 4.15). This demonstrates the possibility of recognizing process deviations to provide an opportunity to adjust parameters (e.g., flowrates) in real time during a run. Once models are developed (as discussed in Section 4.1.4), they can be automated using an online monitoring software or Python in future runs.

Table 4.5. Sm^{3+} and Nd^{3+} concentration profiles during the first profile at 9:30 a.m.

Stage	Nd mM (aqueous)	mM Sm (organic)
1	0	7.034
2	NA	6.810
3	0	6.592
4	0	6.570
5	0	6.550
6	0.30	6.555
7	0.45	6.756
8	0.77	5.072
9	1.23	7.769
10	2.00	7.775
11	7.63	7.424
12	5.30	4.068
13	3.26	1.778
14	1.28	0
15	0.42	0
16	~0.2	0

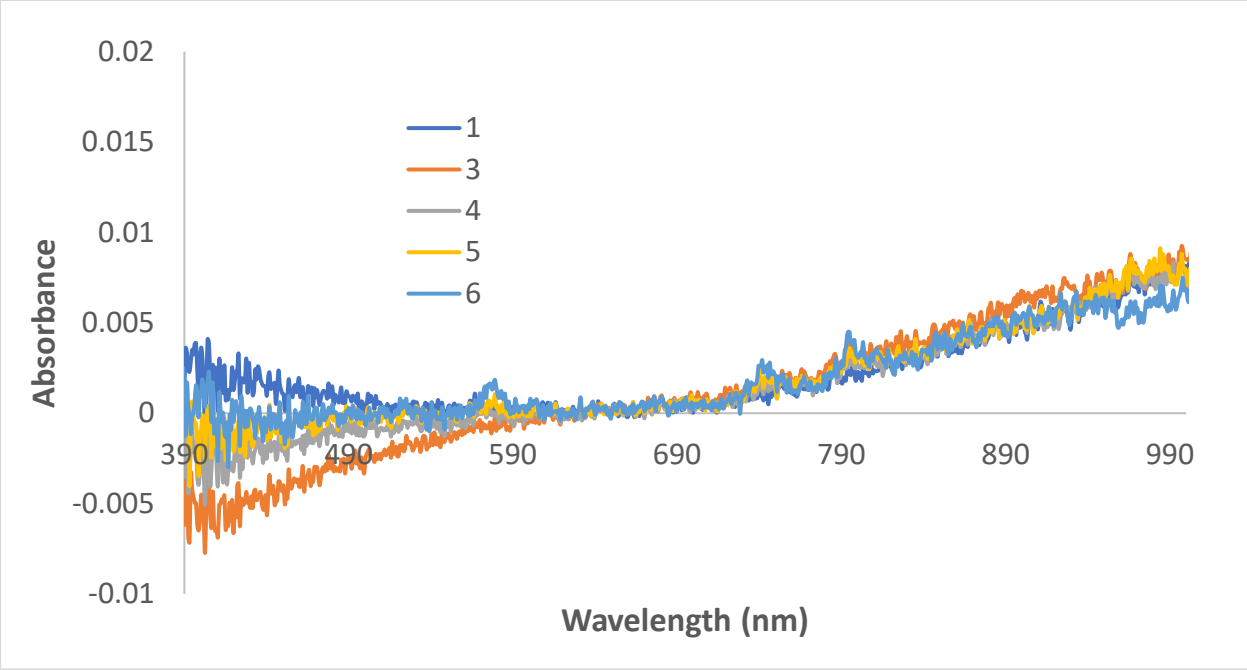

Figure 4.15. Aqueous UV-Vis absorption spectra collected at 9:30 a.m. in Stages 1 and 3–6.

Table 4.6. Sm^{3+} and Nd^{3+} concentration profiles during the second profile at 11:00 a.m.

Stage	Nd mM aqueous	mM Sm organic
1	0.58	NA
2	NA	NA
3	1.38	~0.8
4	1.71	1.78
5	2.00	4.07
6	2.41	7.42
7	2.88	7.77
8	3.40	7.77
9	4.01	6.89
10	4.77	6.76
11	11.13	6.55
12	11.26	6.55
13	10.04	6.57
14	7.85	6.59
15	4.78	~7
16	2.03	~7

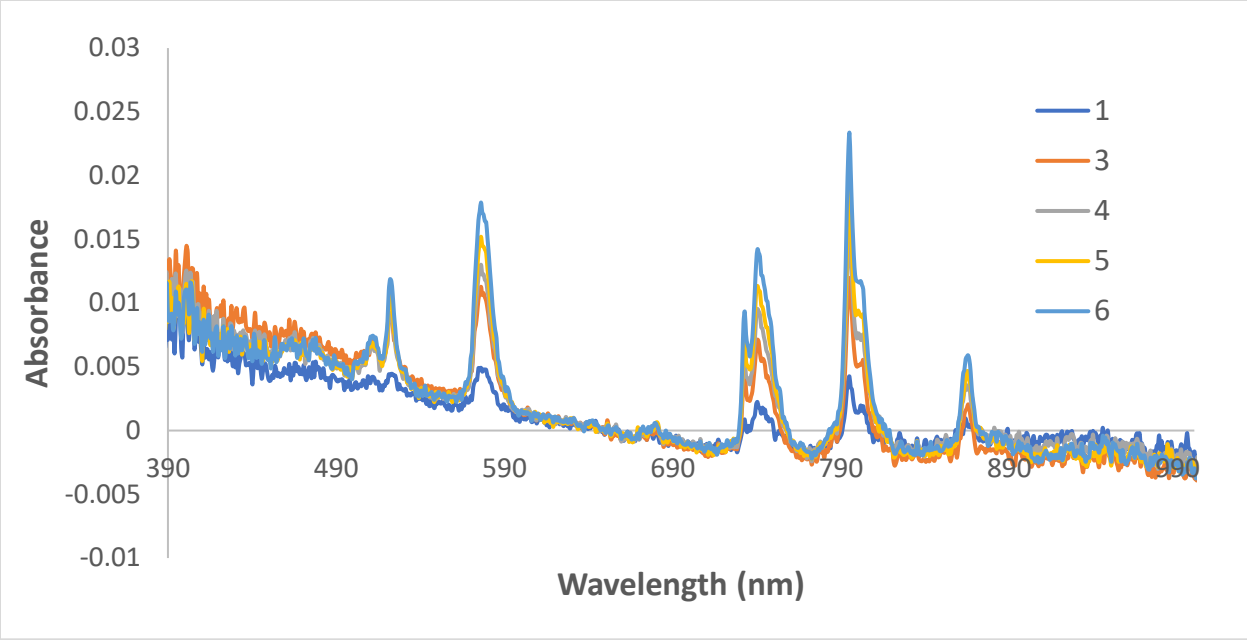

Figure 4.16. Aqueous UV-Vis absorption spectra collected 11:00 a.m. in Stages 1 and 3–6.

4. SAMPLES CONTAINING Pm

4.1 Pm SAMPLE FROM HFIR IRRADIATION

We attempted to measure a Pm absorption spectrum with two samples to approximate molar absorptivity values relative to Nd and compare peak positions to those presented in a report from many years ago [8]. We measured the absorption spectrum of a sample containing Pm and Nd after irradiations at HFIR (Figure 3.1). Sample was prepared in ~2% nitric acid. A first derivative was applied to each spectrum to remove a slight baseline offset.

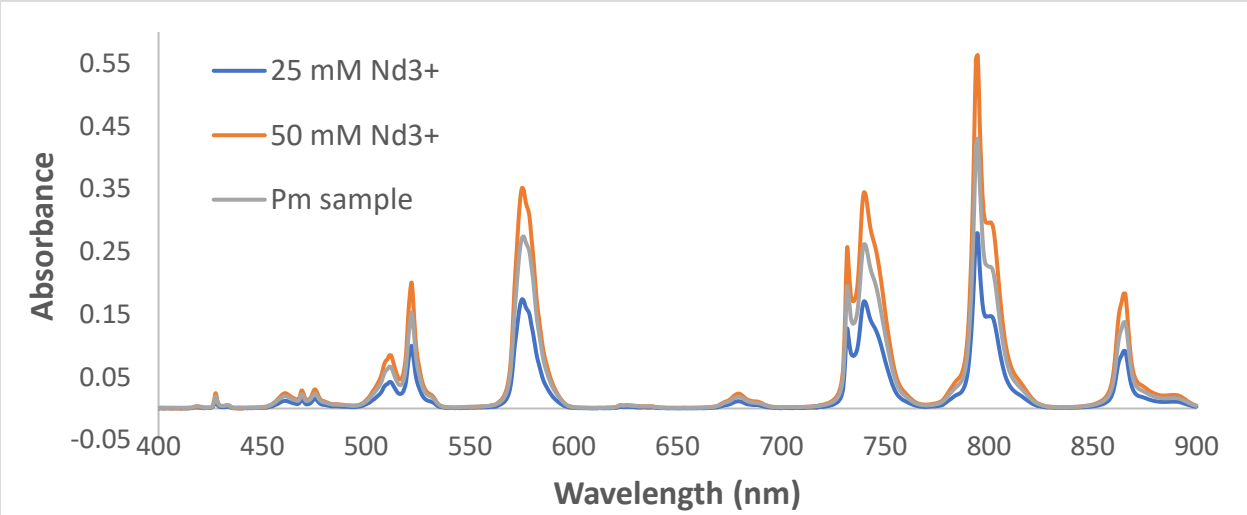

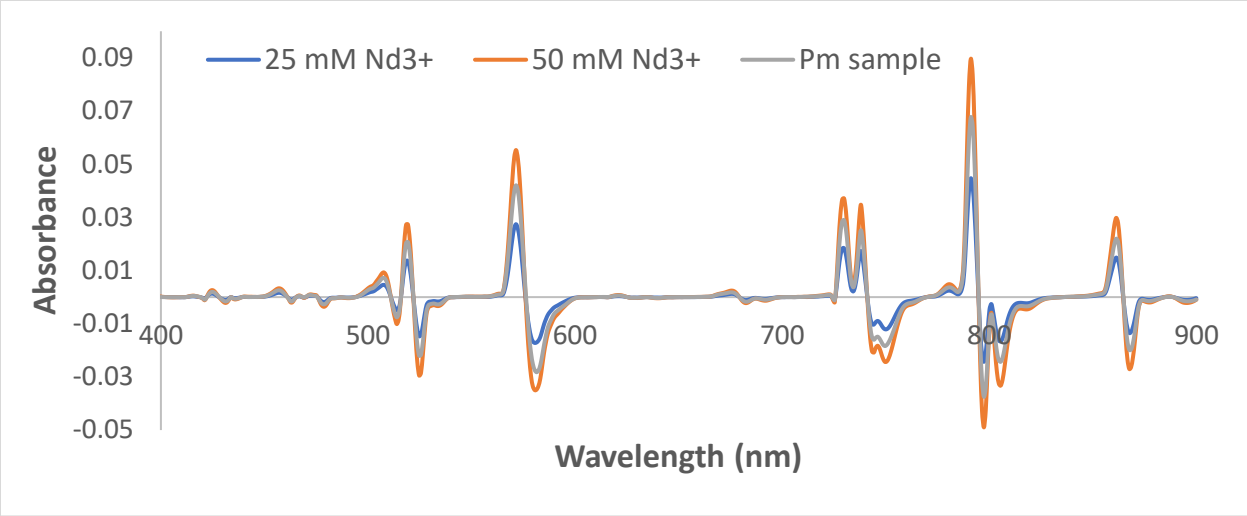

Figure 3.1. Absorption spectra of two Nd^{3+} solutions and the Pm sample (top) and a first derivative applied to the spectra (bottom).

A linear regression of the 791.1 nm peak was used to create curve to determine the concentration of Nd in the Pm sample (Figure 3.2). The spectral response in this concentration range is highly linear (i.e., note R^2 value of 0.999996). The resulting concentration of Nd was 37.8 mM by absorbance spectroscopy. This number agreed with the analytical group. It was slightly lower, possibly due to sample preparation. The sample was diluted slightly in the cuvette because of residual rinse solution that was not removed. Pm^{3+} was not detected in this sample (Figure 3.3). It was outside the detection limits for this technique using cuvette with a 1 cm optical pathlength.

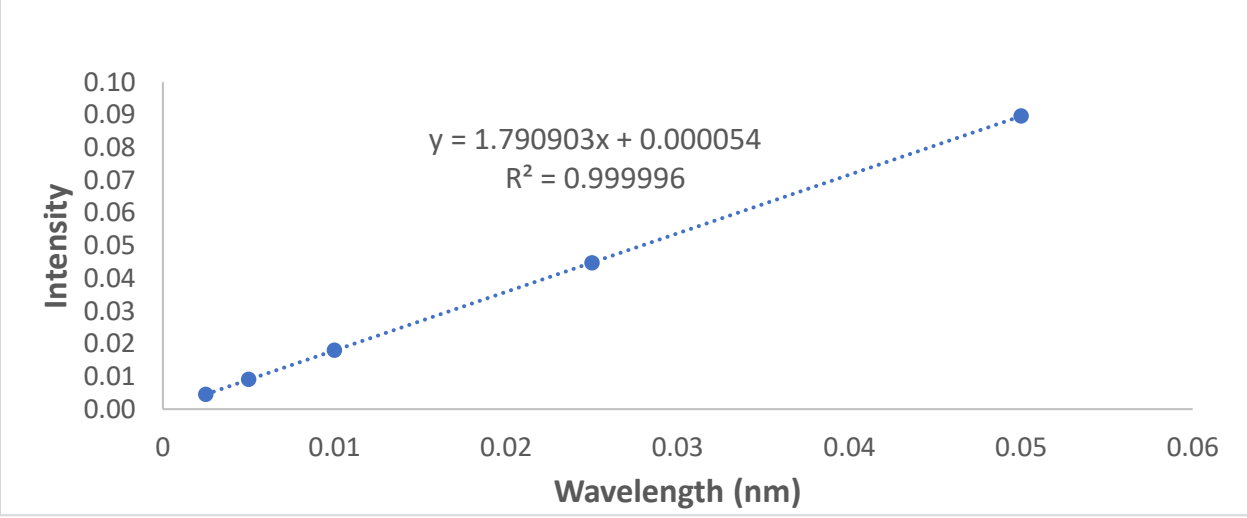

Figure 3.2. Linear regression of the first derivative peak at 791.1 nm peak.

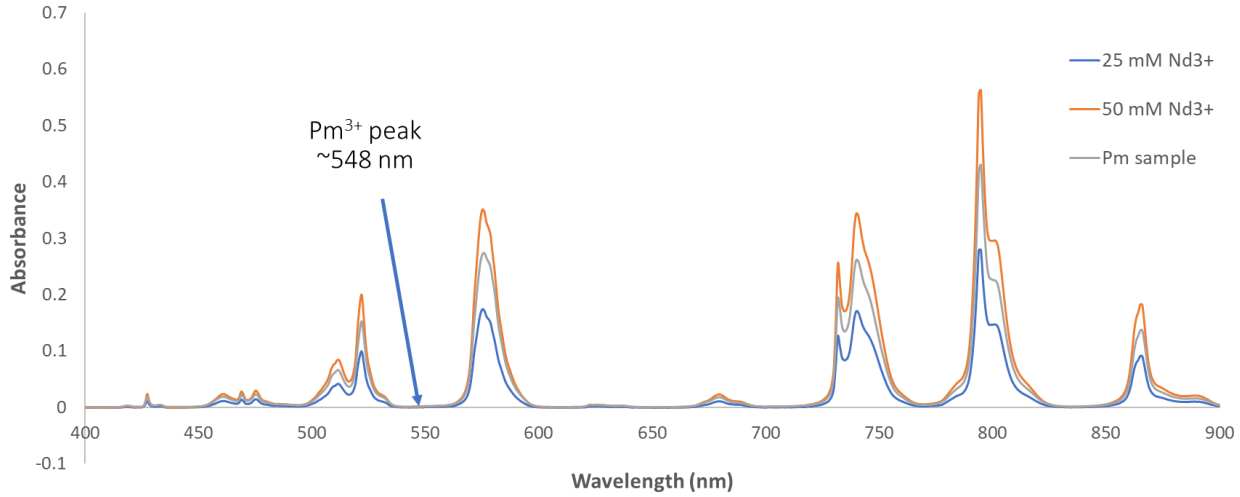

Figure 3.3. Absorbance spectra of Nd samples and the Pm sample. The Pm^{3+} band near 548 nm was not observed (i.e., below detection limits).

4.2 Pm CAVE SAMPLE ABSORPTION SPECTRUM

4.2.1 Example Spectrum and Results

We recorded the absorption spectrum of a sample containing 2.1 Ci ^{147}Pm with a chemical purity of 16% on 12/7/2021. The total lanthanide mass in the sample was 13.93 mg, with a total of 11.7 mg Nd. The sample was dried down and brought up in 1 mL of 1 M HNO_3 to arrive at 15.2 mM Pm^{3+} and 81 mM Nd^{3+}. The solution had a faint purple color, which is indicative of Nd^{3+} (see Figure 3.4). The sample was pipetted into a 1 cm quartz cuvette in rad hood #4 located in Lab 110. A radiological control technician (RCT) surveyed the sample prior to recording an absorption spectrum (350 nm–1,050 nm) at 0.9 nm intervals using the main sample compartment of the Cary 6000i. The spectrophotometer was referenced to deionized water.

Figure 3.4. Sample containing Pm and Nd in a 1 cm quartz cuvette with screw cap.

Pm^{3+} absorption peaks at 494 and 549 nm and a doublet at 700 and 704 nm were clearly identified in the spectrum shown in Figure 3. These peaks were in regions where there are no Nd^{3+} peaks (compare to Figure 3.7). The Pm peaks were consistent with previously reported values [8]. The molar absorptivity values were only approximated here, but they appear to be less than Nd and more comparable to Sm. The small peak near 402 nm in the Pm cave spectrum could be Sm. Attempts to subtract a pure Nd reference spectrum from the convoluted Pm cave sample spectrum were mostly unsuccessful. To subtract the Nd^{3+} contribution from the Pm/Nd cave sample spectrum, the reference 25 mM Nd spectrum was scaled by a factor of 1.35 to match the highest peak intensity at 795 nm. This scaled spectrum would equate to a Nd^{3+} concentration of 34 mM because absorbance and concentration are directly proportional. The Nd^{3+} concentration was much higher: ~81 mM in the Pm sample. Therefore, the molar absorptivity of the 795 nm peak in the Pm cave sample is different from the control. Nd peak overlap with Pm^{3+} peaks cannot explain this large discrepancy. The 866 nm Nd^{3+} peak shape in the Pm cave sample spectrum is also distorted in comparison to the reference Nd^{3+} spectrum. Neither Pm nor Sm absorb light in this region, so the change in shape must correspond to a significant difference in the solute. Additionally, relative Nd peak intensities are different from the reference.

If the solute contained N,N,N′,N′-Tetraoctyl diglycolamide (TODGA) or another impurity, then the Nd absorption spectra may change compared to Nd in pure nitric acid [2]. Finally, the negative water band peak in the ~960 nm region is much more pronounced in the Pm spectrum than the scaled 25 mM Nd spectrum. This suggests that water molecules are much more distorted in this sample. The concentration of acid and lanthanides is comparable between these samples, and the temperature is the same. This implies that the discrepancy must be explained by something else related to the solvent (e.g., ionic strength, TODGA).

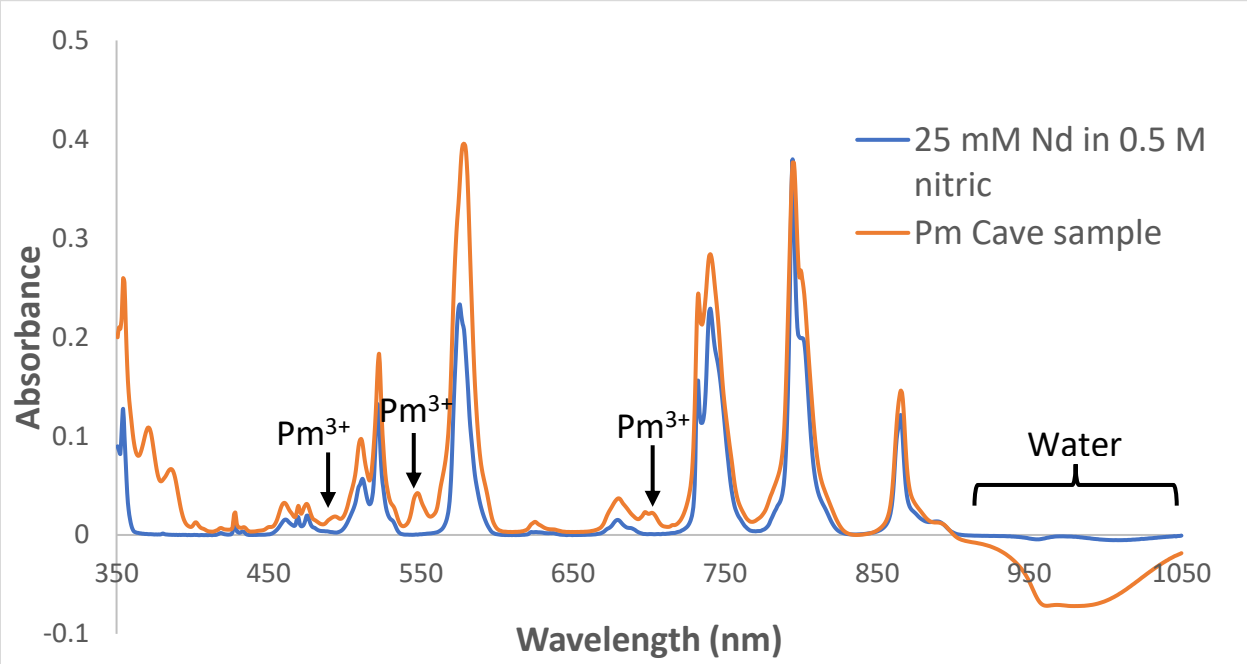

Figure 3.5. Pm sample absorption spectrum compared to a 25 mM Nd solution in 0.5 M nitric acid. The most resolved Pm^{3+} peaks are labeled. The 25 mM Nd spectrum was scaled by a factor of 1.35 to match the intensity of the peak at 795 nm.

A baseline offset correction was applied to the Pm spectrum shown in Figure 3.5 by subtracting the absorbance value at 837 nm from every point in the spectrum. The raw data had a shifted baseline (Figure 3.6). This qualitatively suggests that there could be particulates in the sample. We plan to load cold Nd onto DGA, elute it, and compare the resulting absorption spectrum to the 25 mM reference Nd spectrum. Similarities between a Nd DGA column spectrum and the Pm cave spectrum could imply that TODGA is responsible in part for the differences in Nd spectra.

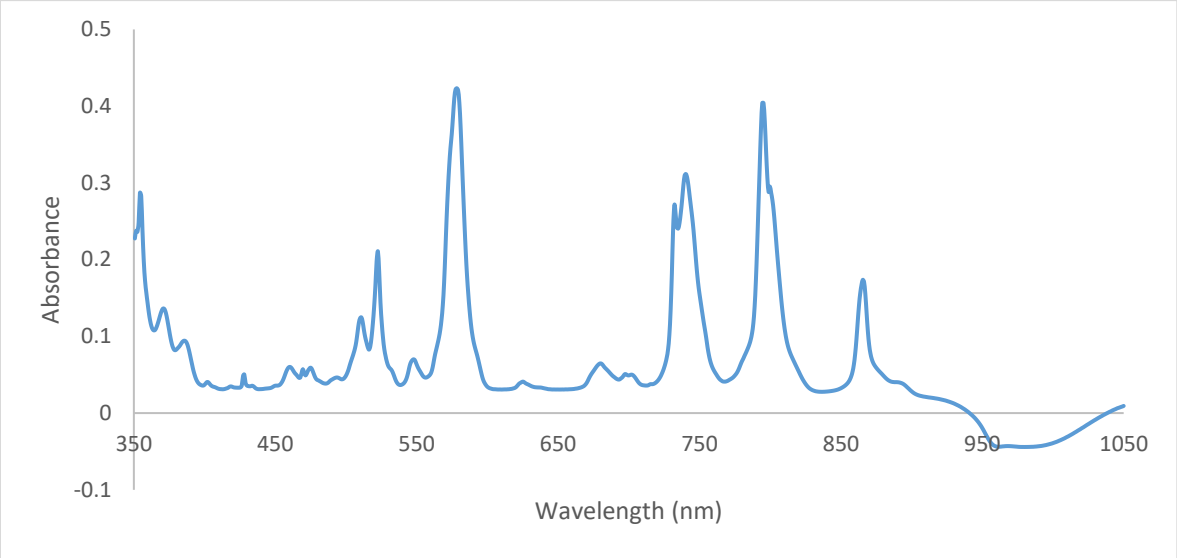

Figure 3.6. Pm cave sample raw absorption spectrum. Note the shifted baseline.

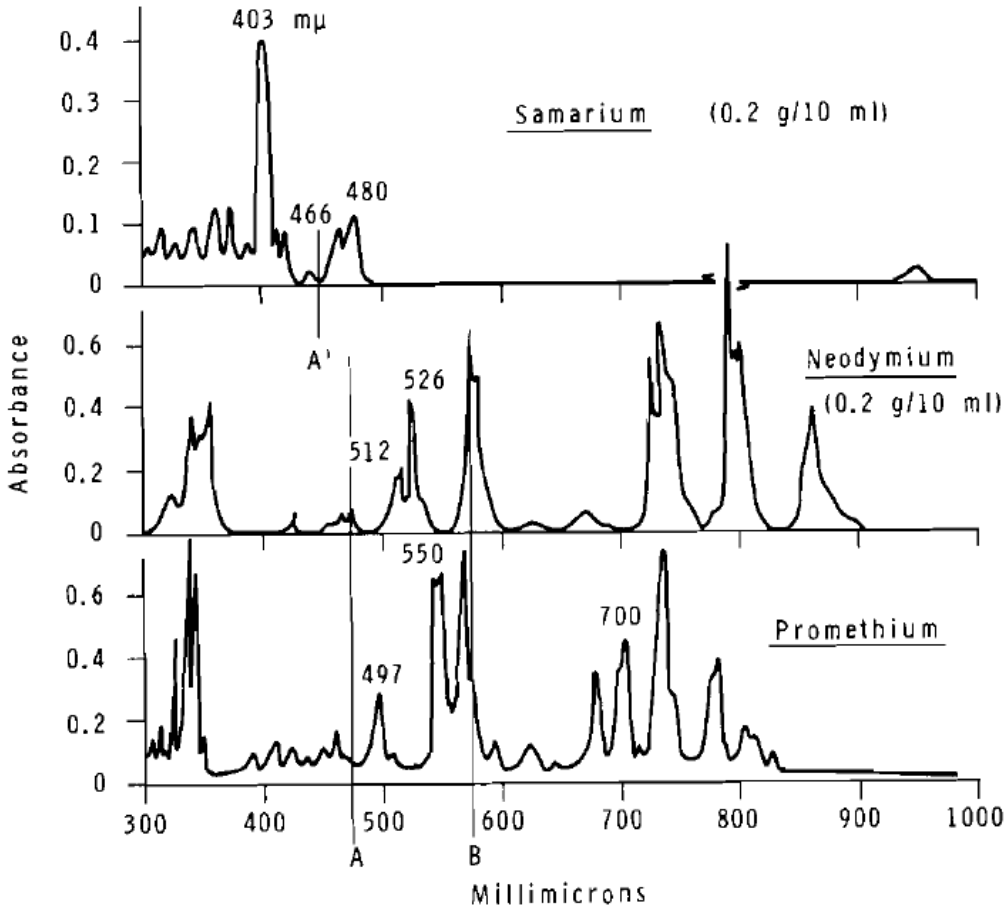

Figure 3.7. Example spectra taken from report BNWL-337 published in 1967 [8].

4.2.2 Isotope Discussion

It is challenging to obtain the concentration of Nd, Pm, Sm, and other analytes in fission product samples because lanthanides have multiple mass numbers, and they tend to overlap. The Pm fission product sample had Nd isotope ratios so different from the model the analytical group at REDC uses that the results could not automatically be assigned to the analytes based on the model. The masses were assigned using calculated expectation. This measurement could be simplified if we can show that it is possible to subtract the Nd background using a natural Nd spectrum. Samples would ideally be prepared in 4% nitric acid or another consistent medium to remove difference from various matrix effects. This would be comparable to how samples are prepared for ICP-OES or inductively coupled plasma–mass spectrometry (ICP-MS).

It is possible to measure hyperfine structure related to isotopes with optical spectroscopy. If isotopic shifts in absorption spectra were that obvious, such an application would have been exploited decades ago. We hypothesize that the shifts are so small they are negligible. Hyperfine structure arises due to interactions between the nucleus and electron clouds. Typically, isotopic shifts are order of magnitude more obvious in vibrational molecular spectra, where these spectra correspond to electronic transitions of atomic spectra. Atomic isotope shifts are often on the order of picometers, it is unlikely that we have the resolution to detect it. Line broadening is such a dominant effect in aqueous solutions at ambient

temperature that those collisional mechanisms create linewidths that are much broader than isotopic shifts.

5. SUMMARY AND MAJOR CONCLUSIONS

5.1 FUTURE STUDIES AND APPLICATIONS

Several items have been identified for future work.

First, it would be useful to consider developing a dual fluorescence and absorption in-line flow cell. Although numerous options are available commercially, they normally do not have a notch filter to block the laser light or a longer pathlength (e.g., 5 cm) optimized for low Pm^{3+} concentration. With this cell, it would be possible to measure the more trace-species Sm^{3+} by the fluorescence signal and Nd or Pm using absorption. This approach would be useful where concentrations are in suitable ranges. Figure 5.1 provides a schematic for a potential flow cell design.

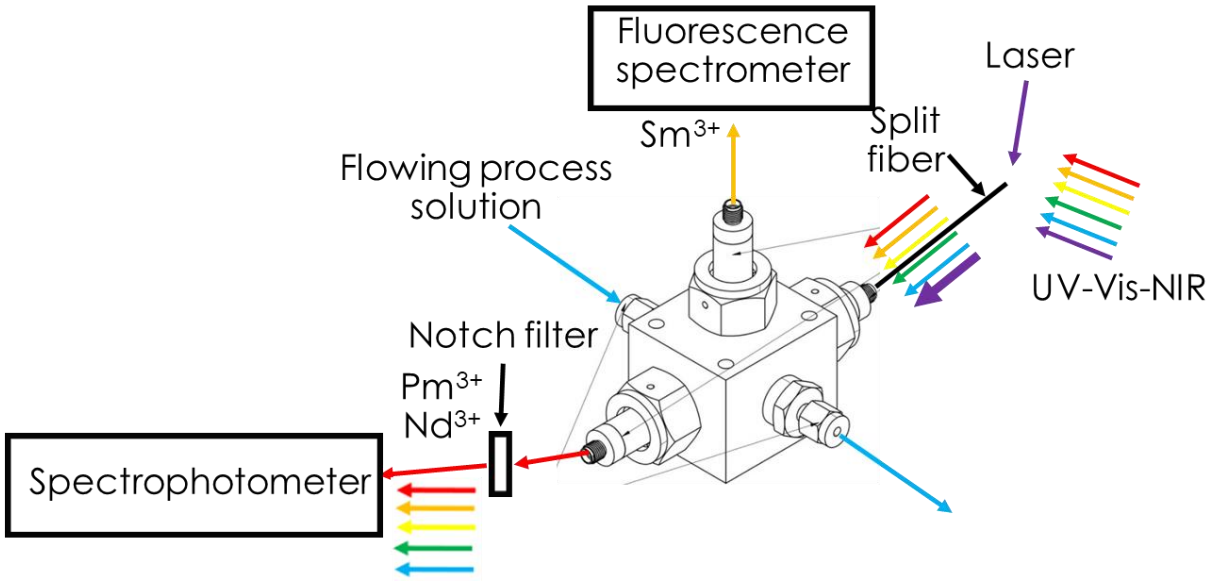

Figure 5.1. Notional schematic for dual fluorescence and absorption flow cell.

Second, it would be interesting to conduct a study focused on collecting spectral training sets corresponding to aqueous- and organic-phase spectra containing Nd and Sm with referencing the spectrophotometer to water only. This would simplify data collection. The convoluted peaks and baseline offsets could be modeled using an appropriate preprocessing strategy and multivariate data analysis (e.g., partial least-squares). The absorbance spectrum of the organic phase after referencing the spectrometer to the aqueous phase is shown in Figure 5.2 for reference.

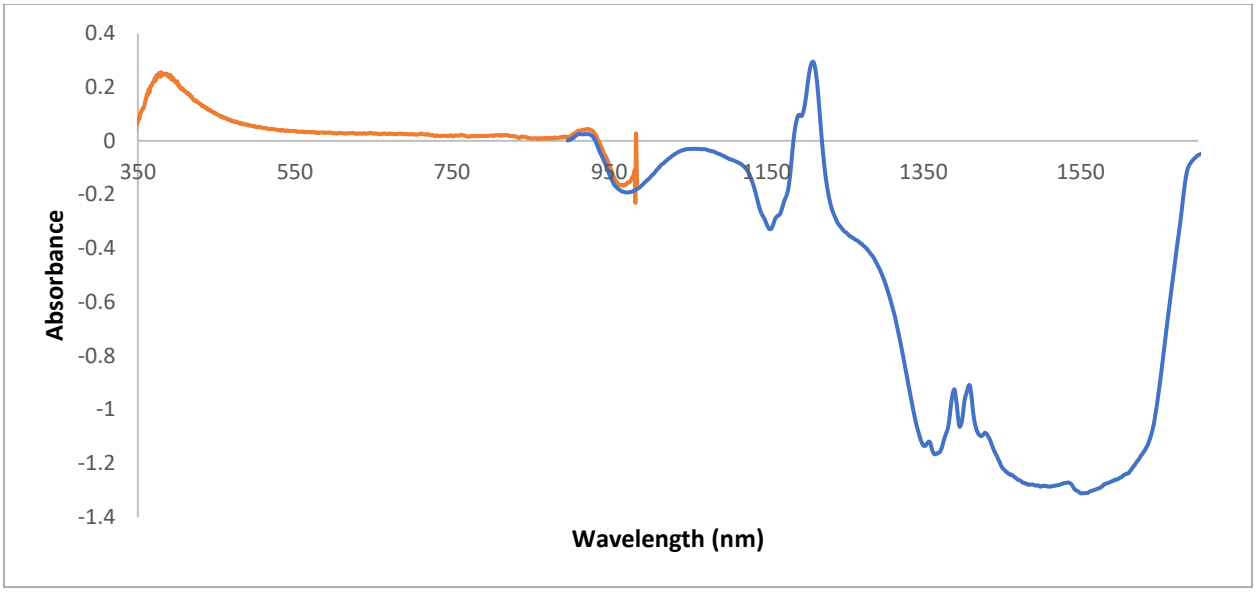

Figure 5.2. Organic-phase spectrum with the spectrometer referenced to the aqueous phase. Note the wavelength region >~1,300 nm is not usable.

Third, longer pathlength flow cell options are commercially available. Custom Sensors and Technology offers options ranging from 75 to 500 mm with multiple port connections and SMA-905 fiber optic connections. These could be placed in-line with the effluent of ion exchange column runs or centrifugal contactors. A longer pathlength cell (e.g., 10 mm) would enhance sensitivity for Pm^{3+} to meet required detection limits.

5.2 CONCLUSIONS

This work describes several proof-of-principle experiments demonstrating the possibility of using spectrophotometry and fluorescence spectroscopy to monitor Sm, Pm, and Nd. Spectrophotometry will be useful for monitoring both the aqueous and organic phases for each analyte at relevant concentrations. Future work could focus on applying real-time monitoring tools during mixer–settler runs using an online monitoring software or Python coding.

REFERENCES

[1] Sadergaski, L. R.; Myhre, K. G.; Delmau, L.; Benker, D.; DePaoli, D.; Wham, R. “Spectroscopic and Multivariate Analysis Development in Support of the Plutonium-238 Supply Program.” In *Nuclear and Emerging Technologies for Space*, 2020.

[2] Sadergaski, L. R.; Myhre, K. G.; Delmau, L. H.; DePaoli, D. W.; Wham, R. W. *Status of Spectroscopy and Online Monitoring for the Plutonium-238 Supply Program.* ORNL Technical Report no. ORNL/TM-2021/1922. Oak Ridge, TN: Oak Ridge National Laboratory, 2021.

[3] Sadergaski, L.; Schwengels, S. S.; Delmau, L. H.; Benker, D. E.; DePaoli, D. W.; Wham, R. M. “Online Monitoring of Radiochemical Processing Streams for the Plutonium-238 Supply Program.” In *Nuclear and Emerging Technologies for Space*, 2021.

[4] Sadergaski, L. R. Schwengels, S. S.; Delmau, L. H.; DePaoli, D. W. *Monitoring Radiochemical Processing Streams for the 238Pu Supply Program with Process Pulse II.* ORNL Technical Report no. ORNL/TM-2021/3. Oak Ridge, TN: Oak Ridge National Laboratory, 2021.

[5] Sadergaski, L. R.; Benker, D. E.; DePaoli, D. W.; Wham, R. M.; Delmau, L. H. *Spectrophotometric Analysis of P5PX-1 to Support the ^{238}Pu Supply Program*. ORNL Technical Report no. ORNL/TM-2021/2317. Oak Ridge, TN: Oak Ridge National Laboratory, 2021.

[6] Sadergaski, L. R.; Patton, K. K.; Toney, G. K.; DePaoli, D. W.; Delmau, L. H. *Measuring Neptunium Concentration Using Optical Spectrometry for the Plutonium-238 Supply Program*. ORNL Technical Report no. ORNL/TM-2021/2072. Oak Ridge, TN: Oak Ridge National Laboratory, 2021.

[7] Sadergaski, L. R.; Myhre, K. G.; Delmau, L. H. "Multivariate Chemometric Methods and Vis-NIR Spectrophotometry for Monitoring Plutonium-238 Anion Exchange Column Effluent in a Radiochemical Hot Cell. *Talanta Open* 5 (2022): 100120.

[8] Upson, U. L.; Wheelwright, E. J. *An In-cell Recording Optical Spectrometer*. BNWL Report no. BNWL-337. Publishing organization city, state: Publishing organization, 1967**.**

[9] Picayo, G. A.; Etz, B. D.; Vyas, S.; Jensen, M. P. "Characterization of the ALSEP Process at Equilibrium: Speciation and Stoichiometry of the Extracted Complex." *ACS Omega* 5 (2020): 8076−8089.

[10] Zhang, P.; Kimura, T. "Complexation of Eu(III) with Dibutyl Phosphate and Tributyl Phosphate." *Solvent Extraction and Ion Exchange* 24 (2006): 149–163.